5-3. Contract Beamlines

BL22XU
JAEA Actinide Science I

1. Introduction

BL22XU is designed to promote basic and applied research on nuclear energy, Fukushima environmental recovery research, 1F decommissioning research, and related research. It was constructed in the storage ring and the RI laboratory of Spring-8 to investigate radioactive materials containing transuranium elements.

BL22XU is characterized by the following two monochromators. One is a cam-type monochromator with a multi-crystal switching system [1]. Si(111) and Si(311) crystals can be arbitrarily switched in a vacuum and in a low-temperature environment. This monochromator generates X-rays of 6–70 keV. The other is a calculated combination monochromator with Si(111) crystals designed for high-flux X-rays of 35–70 keV.

In FY2019, the experimental equipment was relocated and optimized for BL22XU.

2. Experimental hutch 1 (EH1)

2-1. Diamond anvil-cell diffractometer

The diamond anvil-cell diffractometer is designed for both single-crystal and powder X-ray diffraction experiments under high pressure and low temperature. Recently, this diffractometer contributed to the determination of the pressure–temperature phase diagram of a novel perovskite-type oxide $PbCoO_3$, which shows a sequential spin-state transition and intermetallic charge transfer upon applying pressure [2].

This diffractometer was also used for pair-distribution function (PDF) experiments. The PDF measurement system has been improved. The equipped large-area two-dimensional detectors and high-energy monochromatic X-rays are suitable to perform rapid-acquisition PDF experiments. A two-dimensional scattering pattern can be obtained in a short exposure time, which is typically within one minute for a crystalline material. The maximum Q range of the obtained total scattering pattern reaches Q_{max} = 25.5 Å^{-1}, indicating that the spatial resolution of PDF is $\Delta r \sim 0.25$ Å. This is sufficient to discuss the local structure.

The demand for PDF measurements has steadily increased because structural information of functional materials in the local to middle range structures is important to understand the properties. Our PDF system has been applied to investigate various functional materials, including photocatalysts [3], negative thermal expansion materials [4,5], hydrogen-absorbing alloys [6], and cement materials [7].

2-2. Large diffractometer

Currently, an apparatus for Bragg coherent X-ray diffraction imaging (Bragg-CDI) is under development [8]. Bragg-CDI is expected to be a powerful technique for investigating an individual nanosized crystalline particle, and should enable studies of a particle located within devices, which are inaccessible by electron beam techniques.

This technique was used to study particles as

small as ~100 nm in size, which is the most interesting size. Although the experiment was suspended due to the apparatus relocation from EH3 to EH1 in the summer of 2019, it is scheduled to resume once normal operations are restored in the 2020A term.

3. EH3

3-1. Hard X-ray photoemission spectroscopy (HAXPES)

(1) Introduction of the combined dual-mode charge-compensation flood gun

Due to the large electron-escape depths, HAXPES has emerged as a powerful tool for studying both the true bulk and the buried interface properties of complex materials systems. HAXPES has been employed in a wide range of studies.

In insulating material samples, the generation of photoelectrons creates a positive charge in the X-ray irradiation area. Since the spectrum measured in the positively charged state shifts to the side where the binding energy is higher than the actual position, the correct energy position is difficult to grasp. Thus, charge neutralization is necessary during HAXPES measurements of insulating material samples.

In FY2019, HAXPES was equipped with a combined dual-mode charge-compensation flood gun [9]. The dual-beam technique, which simultaneously irradiates a low-energy electron beam and an ion beam, is a neutralization method that stabilizes uneven charges on the surface in a self-repairing manner. This technique can realize stable charge neutralization for a wide range of insulating materials. It has been applied successfully to evaluate the electronic state of insulation samples such as various oxides [10-12].

(2) Ion-irradiation effect of electronic structures in Pt/$Y_3Fe_5O_{12}$ bilayer[12]

Theromoelectric generation using spintronics devices based on the spin Seebeck effect, denoted as the spin-driven thermoelectrics (STEs), offers a novel method of energy conversion from heat into electricity. The separation of heat and charge conduction realizes various devices with simple and flexible structures, low-cost fabrication, etc. Furthermore, spintronics devices generally have a higher tolerance to irradiation damage than semiconductor-based electronics devices. Hence, STE devices are expected to be used in more harsh environments.

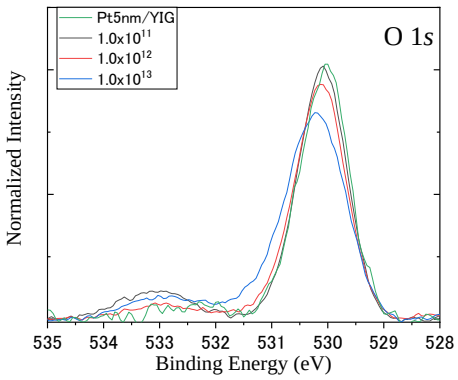

Fig. 1 1*s* HAXPES spectra for Pt/ YIG irradiated with 320-MeV gold-ion beams at various dose levels.

HAXPES measurements were performed to elucidate the ion-irradiation effects at the interface of a typical STE sample, Pt/$Y_3Fe_5O_{12}$ (Pt/ YIG) junction. Various peaks such as Fe 1*s*, Fe 2*p*, O 1*s*, Pt 4*f,* and Y 3*d* were observed. Figure 1 shows the spectra in the O 1*s* region for samples irradiated with 320-MeV gold-ion (Au^{24+}) beams for various dose levels (0, 1.0×10^{11}, 1.0×10^{12}, and 1.0×10^{13}). The binding energies increased with the irradiation

dose level. The binding energies of Fe $2p_{3/2}$ showed similar behaviors, while those of Pt 4*f* did not change. The same tendency was previously reported in the sputtering-damaged interfaces [11], indicating that the interface chemical reaction might be enhanced by ion-beam irradiation.

3-2. Kirkpatrick-Baez (KB) mirror

A KB mirror–focusing system was introduced to analyze cesium-containing microspheres (Cs balls) or fuel debris made by the Fukushima Daiichi Nuclear Power Plant accident. Table 1 shows the KB mirror specifications. In EH3, at 116 m from the light source, micro X-ray fluorescence mapping and micro XAFS measurement can reveal the element distribution, local structure, and chemical bond of the Cs balls and the simulated molten core concrete interaction (MCCI).

The incident X-rays from a front-end slit with a 0.8-mm height and a 1-mm width are monochromatized using a Si(111) double-crystal monochromator (DCM) at 50 m from the light source (Fig. 2). A virtual light-source slit just downstream of the DCM limits the size to a 0.1-mm width. The intensity of the fluorescence X-rays from the sample was measured using a silicon drift detector (Amptek Fast SDD). X-ray fluorescence mapping and XAFS spectra were obtained by scanning the sample position and the incident X-ray energy. A common mirror-control stage was used, and only the mirrors were replaced. Focused sizes of FWHM were around 0.8 μm^2 by each mirror. Then intensities of 10^{11} photons/sec at 15 keV and 10^9 photons/sec at 37 keV were obtained.

Table 1 Mirror specification

Mirrors for low energy (< 16 keV)		
Focusing direction	Vertical	Horizontal
Coat	Rh	
Length	200 mm	300 mm
Glancing angle	3.5 mrad	3 mrad
Working distance	500 mm	
Aperture	630 μm	840 μm
Mirrors for high energy (< 40 keV)		
Focusing direction	Vertically	Horizontally
Coat	Pt	
Length	200 mm	300 mm
Glancing angle	1.7 mrad	1.7 mrad
Working distance	500 mm	
Aperture	306 μm	476 μm

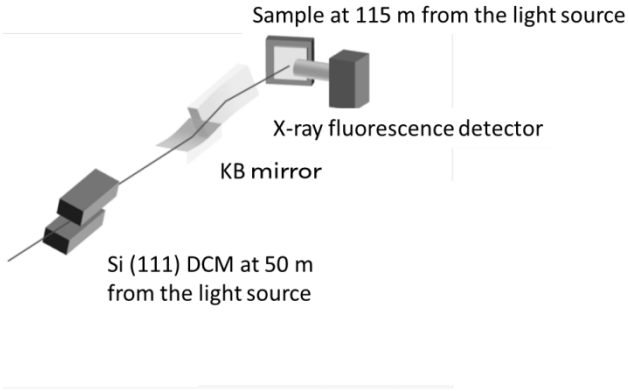

Fig. 2. Experimental layout.

3-3. X-ray absorption fine structure (XAFS)

The interaction and reaction dynamics of heavy-metal ions such as actinides in various environments have been investigated using the XAFS system. This research has contributed to the development of new separation methods on radioactive waste disposal, waste volume reduction, improved reliability in disposal processes, etc. In addition, the knowledge obtained from this

research will also contribute to the development of separation methods for rare metals.

Our previous studies revealed that a heterodonor ligand PTA recognizes slight differences in the ionic sizes of actinides and lanthanides, and separates specific elements as precipitates. Elucidating the reaction method should improve this separation method. Thus, an *in situ* observation system was constructed using time-resolved XAFS to clarify structural changes in the reaction and precipitation process. In this system, a reaction cell that can control a chemical reaction is installed in the existing XAFS system on the experimental EH3 of BL22XU, and time-resolved measurements are performed by the Quick-XAFS method. In the reaction cell, syringes and tubes for dropping two different solutions are connected to the sample container, and the syringe pumps are remotely operated from outside the experimental hutch during XAFS measurements.

Using this system, PTA and some separation reagents were added to a mixed solution of trivalent lanthanides, and the structural changes in the complexes during precipitation were successfully observed. It was revealed that the ligand rapidly interacted with the lanthanide ion, but then precipitated with a gradual structural change over time.

3-4. Stress and imaging measurements

In this device, deformation and state changes inside a material can be performed by a diffraction method and an imaging method using high-energy synchrotron radiation X-rays. Recently X-ray imaging measurements with a time resolution of 1 msec have been used to evaluate processing techniques.

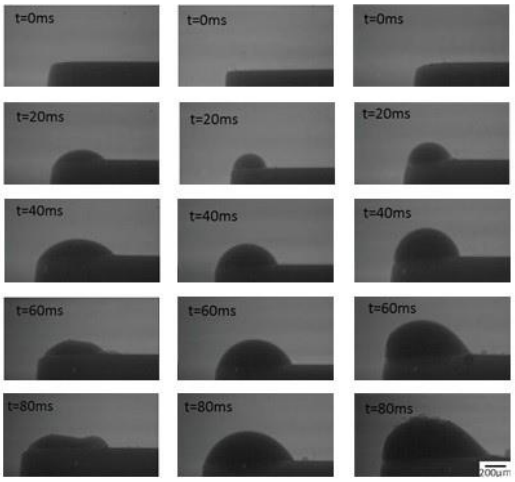

(a)14 mg/s (b)50 mg/s (c)80 mg/s

Fig. 3. Pure copper layer formation investigated by X-ray imaging.

Figure 3 shows the process of layer formation every 20 ms from 0 ms to 80 ms under blue-laser irradiation when a pure copper powder supply on SUS304 stainless steel is varied 14, 50, and 80 mg/s [13]. A clean hemisphere was formed under all conditions up to 40 ms. After 40 ms, a wavy surface was formed at a condition of powder supply of 14 mg/s, and a lot of powder remained on the surface at the condition of powder supply of 80 mg/s. On the other hand, at a condition of powder supply of 50 mg/s, the spread in the horizontal direction was reduced, and the powder was stacked in the upward direction, and thick pure copper layer formation was confirmed. In this experiment, the substrate was moved at a scanning speed of 10 mm. Under these conditions, we inferred that the optimal condition to form a clean film was a 50 mg/s of powder supply and a liquid-temperature state, which maintains the hemisphere.

3-5. K-type Diffractometer

The Kappa diffractometer was moved from the BL14B1 to BL22XU in the RI experimental building to integrate the equipment into the RI experimental building (Fig. 4). The K-type diffractometer has been used for surface X-ray diffraction and high-energy X-ray diffraction experiments. In addition, BL22XU will also support research unique to the RI experimental building.

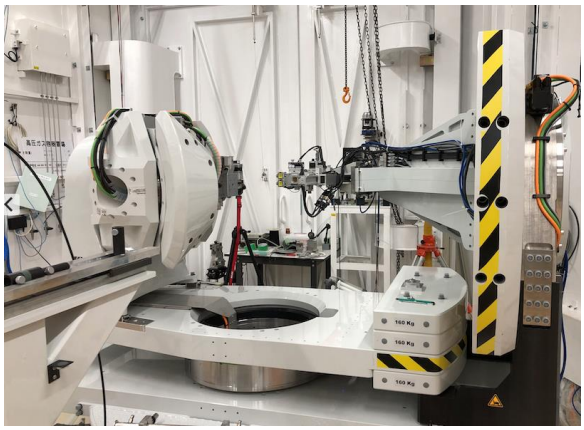

Fig. 4. K-type diffractometer relocated to BL22XU.

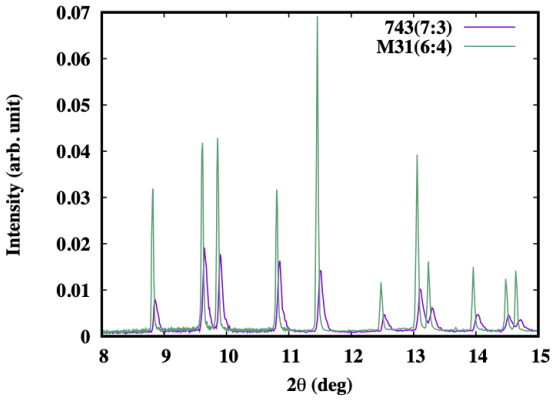

Fig. 5. Powder X-ray diffraction pattern measured by the transmission of a mixed pellet of UO_2 and ZrO_2. UO_2 is easily oxidized and unstable, but the entire pellet can be evaluated using the permeation method.

In the future, the characteristics of simulated debris containing uranium oxide will be evaluated. In fact, studies on actual debris are scheduled in the near future.

Hideaki Shiwaku[*1], Akihiko Machida[*2], Kenji Ohwada[*2], Masaaki Kobata[*1], Tatsuo Fukuda[*1], Kenji Yoshii[*1], Hajime Tanida[*1], Tohru Kobayashi[*1], Takahisa Shobu[*1], and Yasuhiro Yoneda[*1]

[*1] Japan Atomic Energy Agency

[*2] National Institutes for Quantum and Radiological Science and Technology

References:

[1] H. Shiwaku et al., *AIP Conference Proceedings* 705, 659 (2004)

[2] Z. Liu et al., *J. Am. Chem. Soc.* 142, 5731 (2020).

[3] Y. Ide et al., *Chem. Sci.* 10, 6604 (2019).

[4] Y. Sakai et al., *Chem. Mater.* 31, 4748 (2019).

[5] T. Nishikubo et al., *J. Am. Chem. Soc.* 141, 19397 (2019).

[6] K. Asano et al., *Inorg. Chem.* 59, 2758 (2020).

[7] S. Bae et al., *Constr. Build. Mater.* 237, 117714 (2020).

[8] K. Ohwada, K. Sugawara, T. Abe, T. Ueno, A. Machida, T. Watanuki, S. Ueno, I. Fujii, S. Wada, Y. Kuroiwa: *Jpn. J. Appl. Phys.,* 58, SLLA05 (2019).

[9] Larson PE, Kelly MA., *J. Vac. Sci. Technol. A.* 16(6), 3483 - 3489. (1998).

[10] M. Kobata et al., *J. Nucl. Mater.,* 498, 387-394 (2018).

[11] M. Kobata et al., *JPS Conf. Proc.*, 011192 (2020).

[12] S. Okayasu et al., *J. Appl. Phys.* , 128, 083902 (2020).

[13] R. Higashino, T. Shobu et al., *Proceedings of SPIE* Vol. 11271, 1127114 (2020).